Supplementary Information

2D Titanium and Vanadium Carbide MXene Heterostructures for Electrochemical Energy Storage

Armin VahidMohammadi[1, #], Wentao Liang[2], Mehrnaz Mojtabavi[3], Meni Wanunu[3,4], and Majid Beidaghi[1,*]

[1] Department of Materials Engineering, Auburn University, Auburn, AL 36849, USA.
[2] Kostas Advanced Nanocharacterization Facility (KANCF), Northeastern University, Burlington, Massachusetts 01803, USA.
[3] Department of Bioengineering, Northeastern University, Boston, Massachusetts 02115, USA.
[4] Department of Physics, Northeastern University, Boston, Massachusetts 0 2115, USA.

[#] Current Address: A. J. Drexel Nanomaterials Institute, Department of Materials Science and Engineering, Drexel University, Philadelphia, PA 19104, USA.

***** Corresponding authors: mbeidaghi@auburn.edu

Hypothetical surface area-matching model

We calculated the presumable composition of the MXene heterostructure in which the surface area of the $Ti_3C_2T_x$ and V_2CT_x would match for a prefect assembly based on a hypothetical surface-area matching model suggested in the literature.[1–3] For these calculations, as it is shown in **Figure S1**, we considered the previously reported approximate a-lattice parameters of ~0.305 nm for the $Ti_3C_2T_x$ [4,5] and ~0.32 nm for the V_2CT_x [6]. Based on these values and the hexagonal in-plane structure of the MXenes, their 2D weight density can be calculated as follows:[1–3]

$$\text{Theoretical 2D weight density (for in-plane hexagonal structures)} = \frac{M_{2D\ Material}}{a^2 \times sin\,(120°) \times N_A}$$

$M_{2D\ Material}$: Molecular weight of the material (g mol^{-1})

a: a-lattice parameter

N_A: Avogadro number

$$\text{For } Ti_3C_2T_x\text{: } W_{Ti_3C_2T_x} = \frac{199.6}{(0.305)^2 \times sin\,(120°) \times 6.02 \times 10^{23}} = 1.23 \times 10^{-20}\ \text{g nm}^{-2}$$

$$\text{For } V_2CT_x\text{: } W_{V_2CT_x} = \frac{145.87}{(0.32)^2 \times sin\,(120°) \times 6.02 \times 10^{23}} = 8.15 \times 10^{-21}\ \text{g nm}^{-2}$$

Therefore, the weight ratio between $Ti_3C_2T_x$ and V_2CT_x would be:

$$\frac{m_{Ti_3C_2T_x}}{m_{V_2CT_x}} = \frac{W_{Ti_3C_2T_x}}{W_{V_2CT_x}} = \sim 1.5$$

This corresponds to a $Ti_3C_2T_x$:V_2CT_x weight ratio of ~60:40.

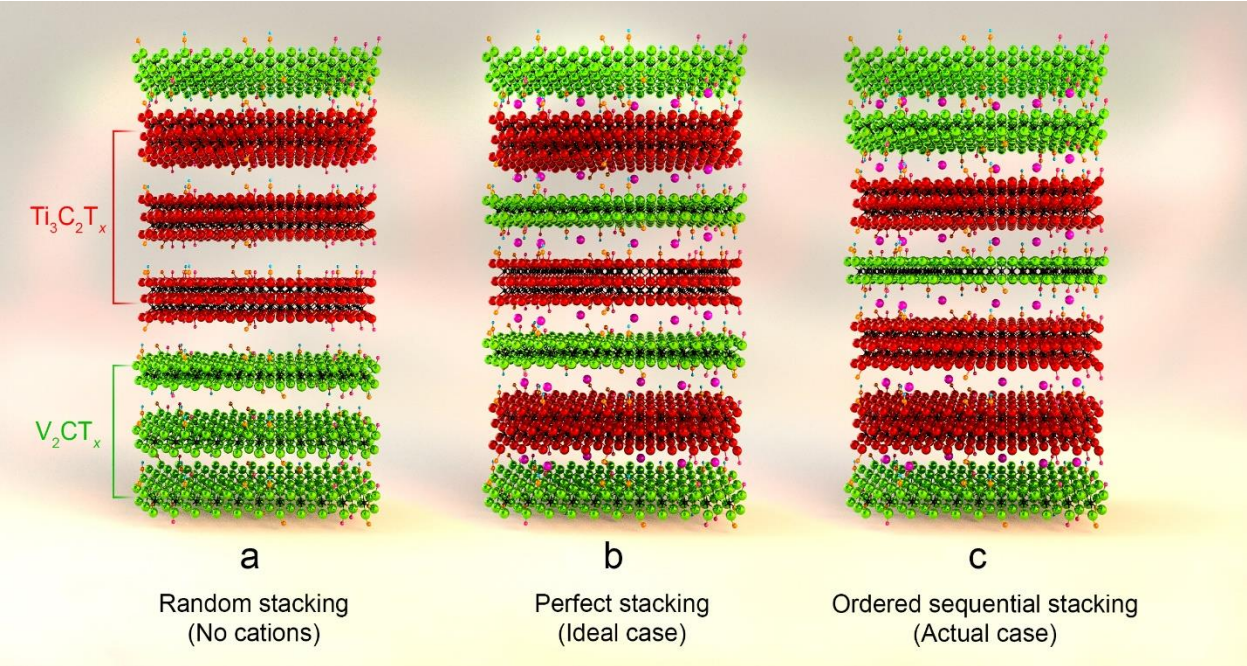

Figure S1. Schematic illustration of the structure of heterolayered MXenes with (a) random stacking and (b, c) ordered sequential stacking.

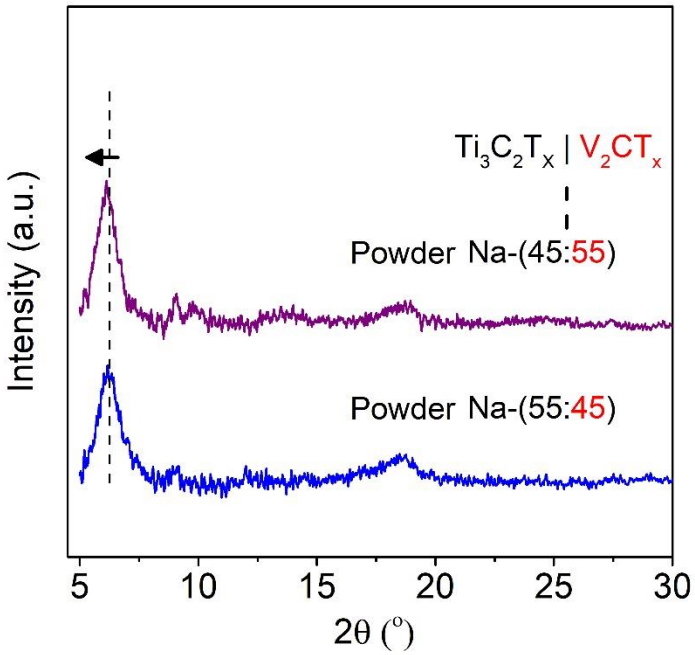

Figure S2. XRD patterns of the heterolayered MXene powders. When the heterolayered MXenes were collected from the top of filter paper and crushed into fine particles, their XRD patterns did not show the presence of separated (000*l*) basal plane peaks for each of the phases and generally the single low angle peak showed lower intensity compared to randomly mixed films (Figure S3). This suggests that there is no phase separation between $Ti_3C_2T_x$ or V_2CT_x MXenes in the hetero powders. Therefore, we assume in the freestanding films prepared by vacuum filtration, the directional ordering of several stacks of the heterolayered flakes during the vacuum filtration yields distinguished (000*l*) basal plane peaks in the XRD patterns.

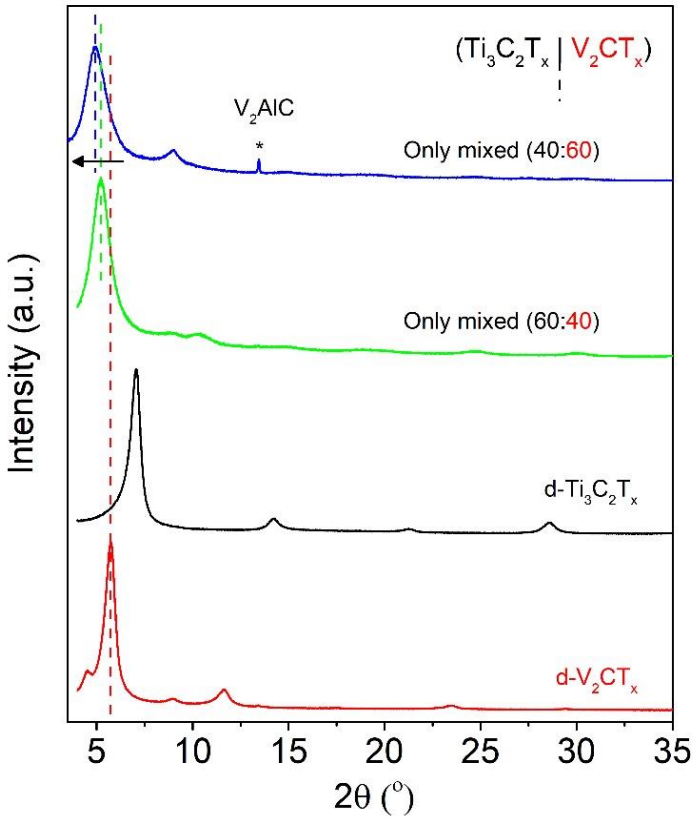

Figure S3. XRD patterns of the MXene mixture films prepared using mixtures of aqueous solutions of $Ti_3C_2T_x$ and V_2CT_x in two different weight ratios of 60:40 and 40:60 compared to films fabricated by the as-prepared dispersions of delaminated MXenes flakes. All films were prepared by vacuum-assisted filtration of their corresponding dispersions. Unlike the heterostructures films prepared by the cation-assembly process, films prepared only by mixing the two different MXenes did not display two different peaks corresponding to (0002) basal planes of $Ti_3C_2T_x$ and V_2CT_x. Instead, only one (0002) peak shifted toward lower angles was observed, which probably originates from random mixing of these two MXenes in the film structure. This suggests that in heterolayered flakes, presence of alternating stacks of Na-V_2CT_x avoids arrangement of larger stacks of $Ti_3C_2T_x$, lowering the intensity of their basal plane peak in the XRD pattern, and therefore, allowing the XRD peak for basal planes of V_2CT_x to be observed in the films.

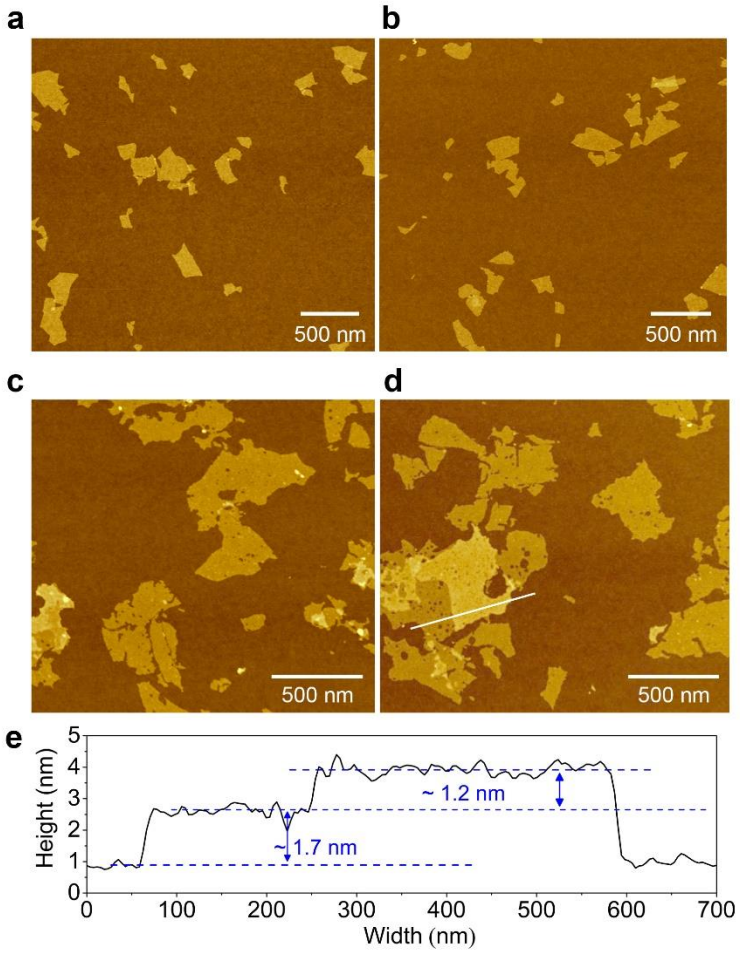

Figure S4. AFM images of (a and b) *d*-$Ti_3C_2T_x$ and (c and d) *d*-V_2CT_x, and (e) the corresponding height profile of the d-V_2CT_x on silicon substrates for the line shown in panel d. Similar to previous reports on $Ti_3C_2T_x$ the exaggerated AFM measured thickness of the *d*-V_2CT_x on silicon reduces to around 1.2 nm when the measurement is done on flakes placed on top of each other.

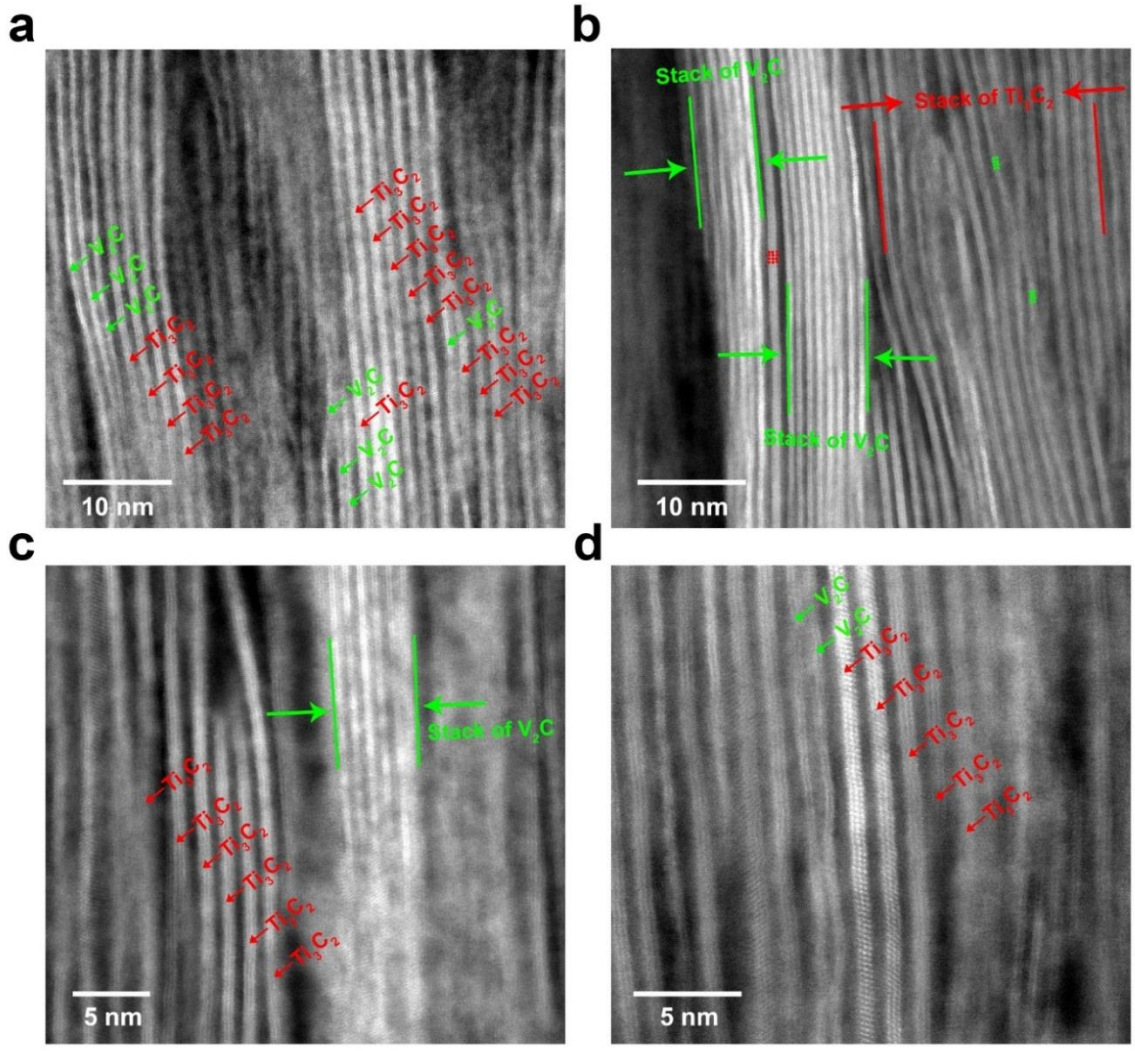

Figure S5. a-d) STEM images of a 60:40 $Ti_3C_2T_x$ to V_2CT_x MXene mixture film produced by vacuum-assisted filtration (without using cations). These images suggest simple mixing results in a random mixture of these two MXene flakes. Large piles of stacked V_2CT_x or $Ti_3C_2T_x$ are marked on these images which show the difference between the flakes stacking in the mixture film and the MXene heterostructures prepared by cation-induced assembly. It is noteworthy that in the mixed film, since V_2CT_x flakes were not assembled using cations, they were very unstable under the TEM electron beam and could be easily damaged by a few seconds of exposure.[7] Therefore, in most areas these flakes appear cloudy and blurry in these images, in contrast to cation-assembled heterostructures where individual V_2CT_x flakes could be better observed.

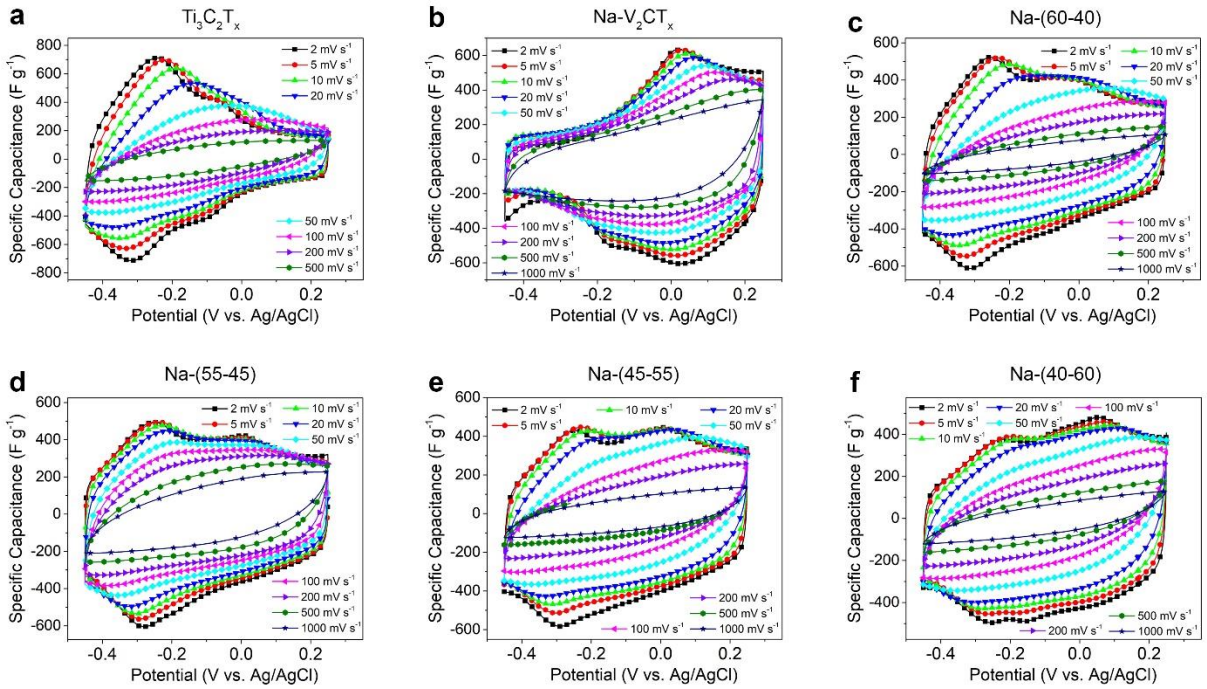

Figure S7. CV profiles of the different freestanding electrodes in 3 M H_2SO_4 at scan rates of 2 mV s^{-1} to 1000 mV s^{-1}. a) *d*-$Ti_3C_2T_x$, b) Na-V_2CT_x, and MXene heterostructure film electrodes with $Ti_3C_2T_x$ to V_2CT_x weight ratio of c) Na-(60-40), d) Na-(55-45), e) Na-(45-55), and f) Na-(40-60).

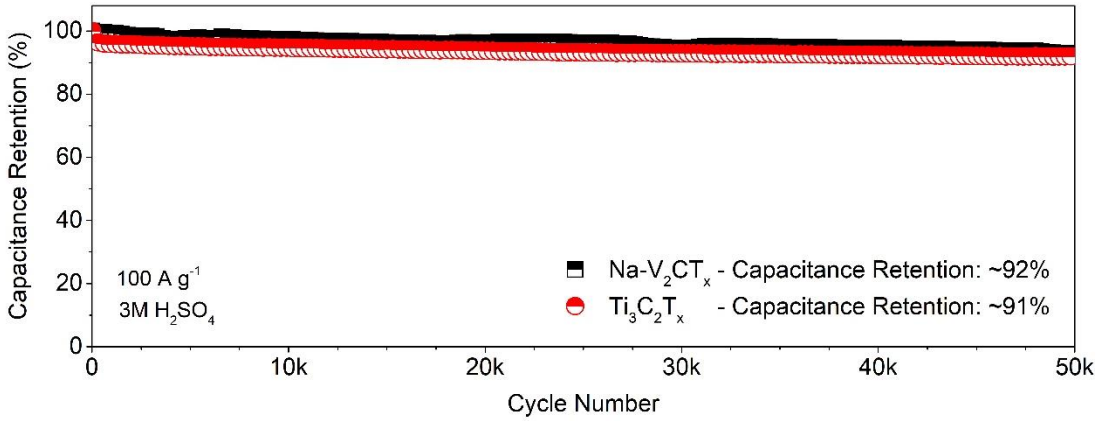

Figure S8. Cycle life of $Ti_3C_2T_x$ and Na-V_2CT_x electrodes in the 3M H_2SO_4 electrolyte at a current density of 100 A g^{-1}.

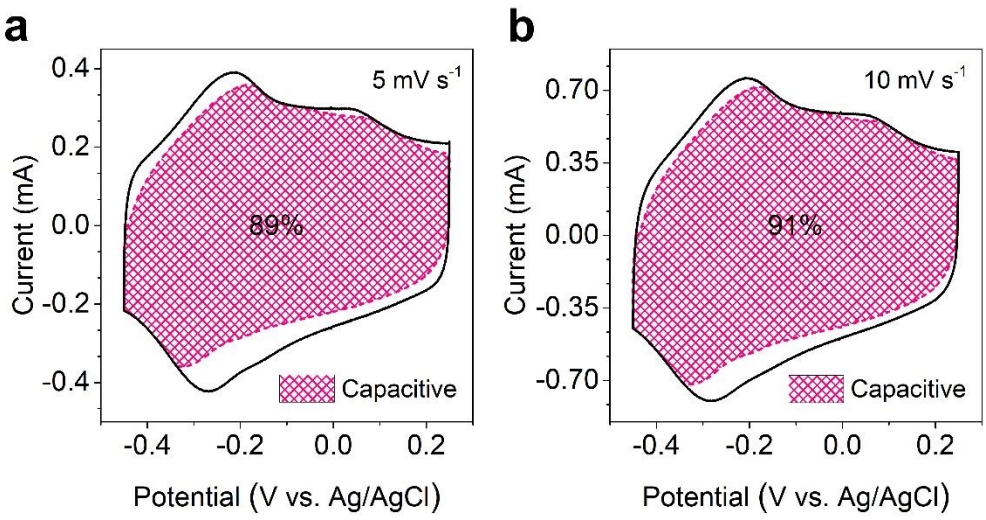

Figure S9. Analysis of the capacitive charge storage contributions from the Na-(50-50) MXene heterostructure at different scan rates of a) 5 mV s^{-1} and b) 10 mV s^{-1}. Hatched portions on the graphs show the surface-controlled (capacitive) contributions.

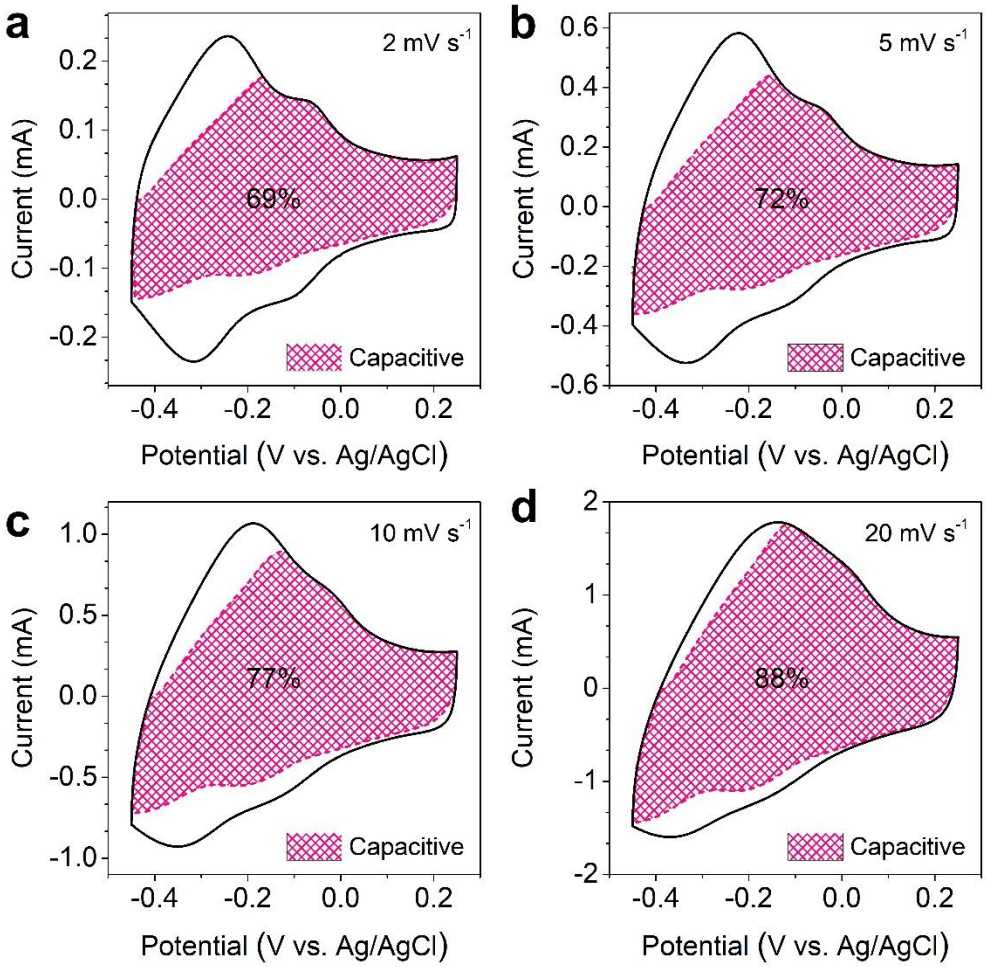

Figure S10. Analysis of the capacitive charge storage contributions from the CV for *d*-$Ti_3C_2T_x$ at different scan rates of a) 2 mV s^{-1}, b) 5 mV s^{-1}, c) 10 mV s^{-1}, and d) 20 mV s^{-1}. Hatched portions on the graphs show the surface-controlled (capacitive) contributions.

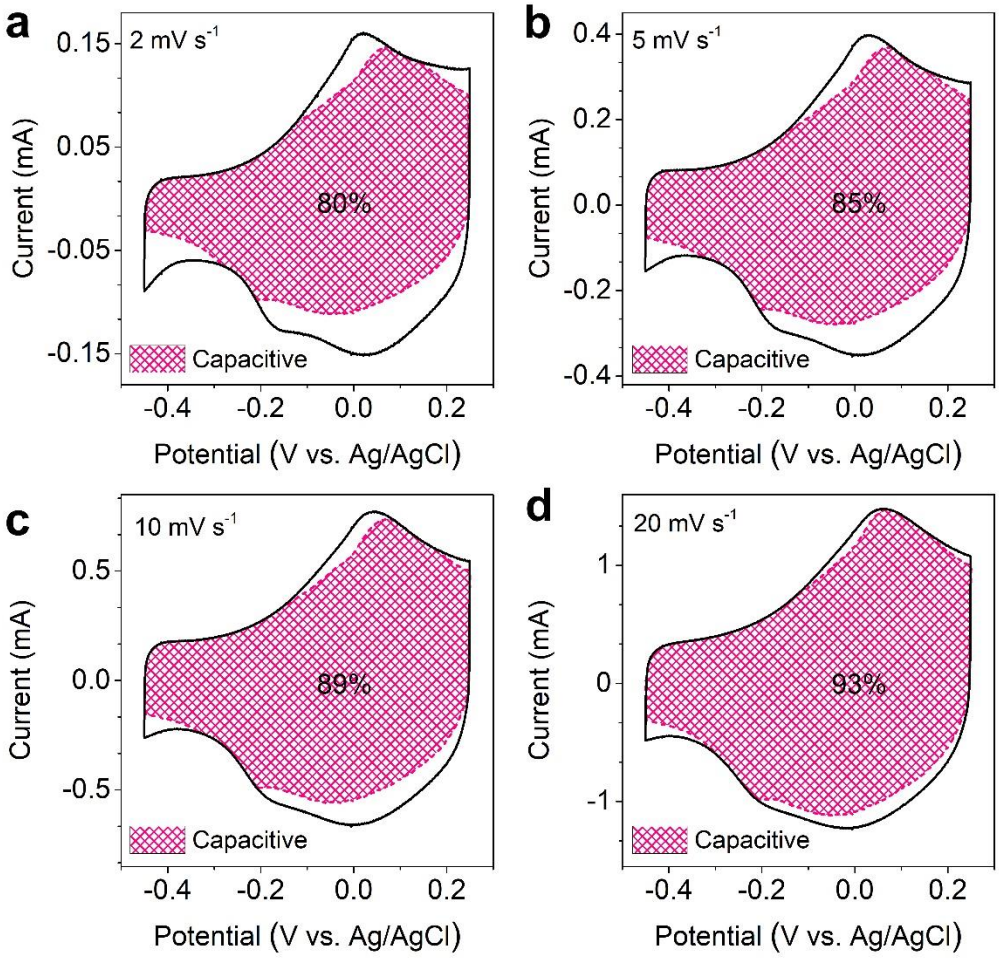

Figure S11. Analysis of the capacitive charge storage contributions from the CV for Na-V_2CT_x at different scan rates of a) 2 mV s^{-1}, b) 5 mV s^{-1}, c) 10 mV s^{-1}, and d) 20 mV s^{-1}. Hatched portions on the graphs show the surface-controlled (capacitive) contributions.

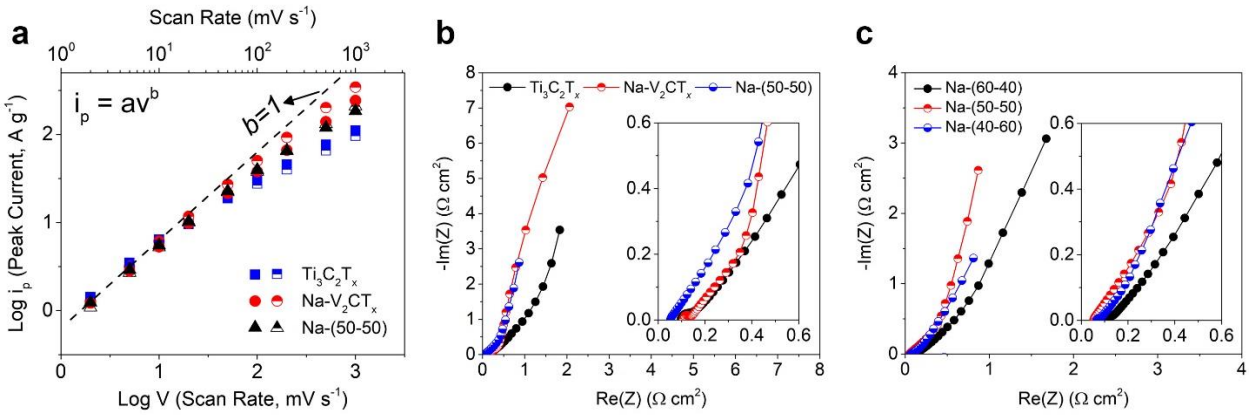

Figure S12. a) Logarithm of cathodic (solid symbols) and anodic (half-filled symbols) peak currents at logarithm of scan rates from 2 mV s^{-1} to 1000 mV s^{-1} for $Ti_3C_2T_x$, Na-V_2CT_x, and Na-(50-50) heterostructure electrodes with comparable thicknesses. In parallel to CV charge analyses, the heterostructure film showed an improved capacitive performance at scan rates higher than 100 mV s^{-1} compared to pristine $Ti_3C_2T_x$ electrode with a similar high rate capacitive performance to that of already promising Na-V_2CT_x.[7] b) Electrochemical impedance spectroscopy (EIS) results for $Ti_3C_2T_x$, Na-V_2CT_x, and Na-(50-50) heterostructure electrodes. As it can be seen from the lower frequency region, the heterostructure electrode showed improved ionic transport properties. c) EIS results for heterostructure electrodes with different compositions. As it can be seen in the graphs, all electrodes showed similarly improved ion transport properties compared to those of individual pristine MXene electrodes. The slightly different increases in the imaginary resistances (corresponding to ion-transport properties) at the high frequency regime for different electrodes could originate from the differences in their thicknesses. As indicated in the paper and known in literature, freestanding MXene electrodes prepared by vacuum filtration usually show a thickness-dependent performance. Nevertheless, heterostructure electrodes could deliver improved capacitances and rate-performances at thicknesses relatively higher than those of pristine MXene electrodes.

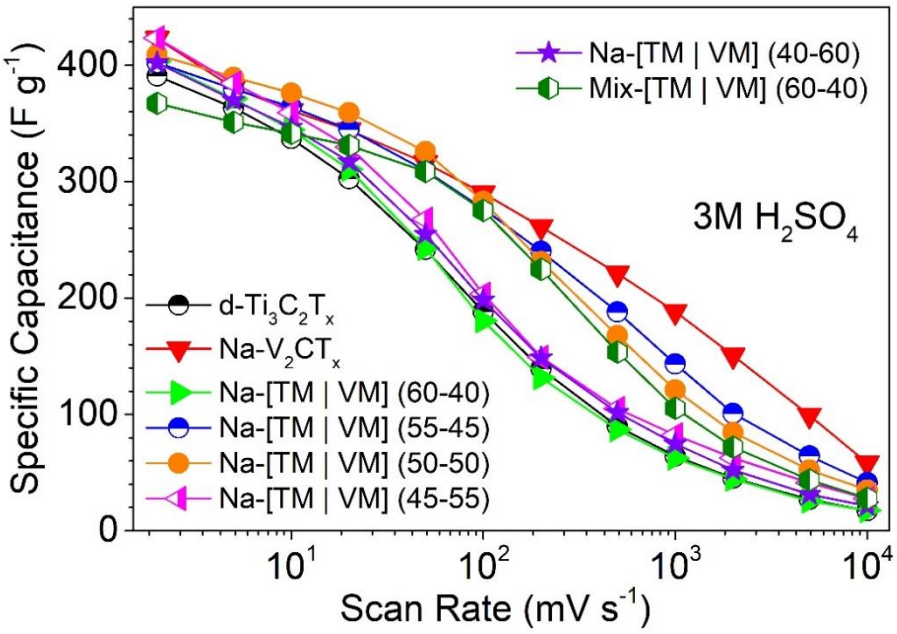

Figure S13. Gravimetric capacitances of different MXene and MXene heterostructure electrodes tested in this experiment as supercapacitor electrodes in 3 M H_2SO_4 electrolyte. TM represents $Ti_3C_2T_x$ MXene and VM represents the V_2CT_x MXene.

References

[1] P. Xiong, R. Ma, N. Sakai, L. Nurdiwijayanto, T. Sasaki, Unilamellar Metallic MoS_2/Graphene Superlattice for Efficient Sodium Storage and Hydrogen Evolution, ACS Energy Lett. 3 (2018) 997–1005. doi:10.1021/acsenergylett.8b00110.

[2] P. Xiong, R. Ma, N. Sakai, T. Sasaki, Genuine Unilamellar Metal Oxide Nanosheets Confined in a Superlattice-like Structure for Superior Energy Storage, ACS Nano. 12 (2018) 1768–1777. doi:10.1021/acsnano.7b08522.

[3] X. Cai, T.C. Ozawa, A. Funatsu, R. Ma, Y. Ebina, T. Sasaki, Tuning the surface charge of 2d oxide nanosheets and the bulk-scale production of superlatticelike composites, J. Am. Chem. Soc. 137 (2015) 2844–2847. doi:10.1021/jacs.5b00317.

[4] C. Shi, M. Beidaghi, M. Naguib, O. Mashtalir, Y. Gogotsi, S.J.L. Billinge, Structure of nanocrystalline Ti_3C_2 MXene using atomic pair distribution function, Phys. Rev. Lett. 112 (2013) 125501. doi:10.1103/PhysRevLett.112.125501.

[5] H.W. Wang, M. Naguib, K. Page, D.J. Wesolowski, Y. Gogotsi, Resolving the Structure of $Ti_3C_2T_x$ MXenes through Multilevel Structural Modeling of the Atomic Pair Distribution Function, Chem. Mater. 28 (2016) 349–359. doi:10.1021/acs.chemmater.5b04250.

[6] A. Champagne, L. Shi, T. Ouisse, B. Hackens, J.C. Charlier, Electronic and vibrational properties of V_2C-based MXenes: From experiments to first-principles modeling, Phys. Rev. B. 97 (2018) 1–11. doi:10.1103/PhysRevB.97.115439.

[7] A. VahidMohammadi, M. Mojtabavi, N.M. Caffrey, M. Wanunu, M. Beidaghi, Assembling 2D MXenes into Highly Stable Pseudocapacitive Electrodes with High Power and Energy Densities, Adv. Mater. 31 (2019) 1806931. doi:10.1002/adma.201806931.